A Nonrigid Registration Framework Using Spatially Encoded Mutual Information and Free-Form Deformations

Xiahai Zhuang*, Simon Arridge, David J. Hawkes, Sebastien Ourselin

***Abstract*—Mutual information (MI) registration including spatial information has been shown to perform better than the traditional MI measures for certain nonrigid registration tasks. In this work, we first provide new insight to problems of the MI-based registration and propose to use the spatially encoded mutual information (SEMI) to tackle these problems. To encode spatial information, we propose a hierarchical weighting scheme to differentiate the contribution of sample points to a set of entropy measures, which are associated to spatial variable values. By using free-form deformations (FFDs) as the transformation model, we can first define the spatial variable using the set of FFD control points, and then propose a local ascent optimization scheme for nonrigid SEMI registration. The proposed SEMI registration can improve the registration accuracy in the nonrigid cases where the traditional MI is challenged due to intensity distortion, contrast enhancement, or different imaging modalities. It also has a similar computation complexity to the registration using traditional MI measures, improving up to two orders of magnitude of computation time compared to the traditional schemes. We validate our algorithms using phantom brain MRI, simulated dynamic contrast enhanced MRI of the liver, and *in vivo* cardiac MRI. The results show that the SEMI registration significantly outperforms the traditional MI registration.**

***Index Terms*—Nonrigid, Registration, Mutual information, Spatial information, Intensity Non-uniformity, Contrast enhancement, Spatially encoded mutual information, SEMI**

I. Introduction

MUTUAL Information (MI) registration, based on information (entropy) theory, assumes a generalized version of *intensity class correspondence* (see Section II-A for detail), instead of intensity value correspondence between the registration images [1]–[3]. This assumption of intensity relation between the images contributes to the wide applicability and good robustness of the MI-based registration [1]–[6]. However, several recent studies have showed that MI-based registration might not be appropriate in certain situations, particularly for nonrigid registration, and encoding spatial information into the MI measures can improve the performance [7]–[13]. The goal of this study is to interpret the problem of MI registration, understand the spatial information encoding in MI registration, and develop an efficient framework for nonrigid registration.

Studholme *et al.* [11] argued that it could be problematic to employ normalized mutual information (NMI) for nonrigid registration of serial brain MRI due to the local intensity changes which are mainly caused by imaging distortions and biological changes of the brain tissue. They proposed to consider the spatial information as an extra channel of information and compute the MI of the three channels as the similarity measure, referred to as regional mutual information (RMI). They validated a derived similarity measure from RMI, denoted as RMI′ in [11]:

$$\begin{aligned}\mathrm{RMI}'(I_r, I_f^T) &= \sum_s p(s) \sum_{r,f} p_s(r,f) \log \frac{p_s(r,f)}{p_s(r)p_s(f)} \\ &= \sum_s p(s) \mathrm{MI}_s(I_r, I_f^T) \ ,\end{aligned} \tag{1}$$

where I_r and I_f^T are respectively the reference image and transformed floating image by transformation T. RMI′ is the linearly weighted sum of a set of local measures $\{\mathrm{MI}_s\}$, and $p(s) = \frac{|\Omega_s|}{\sum_{t=1}^{n_s} |\Omega_t|}$ is proportional to the size of the user-defined local region Ω_s. MI_s is computed within the local region using regional probability distribution functions (PDFs):

$$p_s(r,f) = \frac{1}{N_s} \sum_{x \in \Omega_s} \omega_r(I_r(x)) \omega_f(I_f^T(x)) \ , \tag{2}$$

where ω_r and ω_f are Parzen window functions, N_s is the normalization factor.

Loeckx *et al.* [12], [13] considered the spatial coordinates of sample points in the reference image as *a priori* known conditions and proposed conditional mutual information (cMI) as the similarity measure between the two images:

$$\begin{aligned}\mathrm{cMI}(I_r, I_f^T|s) &= \sum_s p(s) \sum_{r,f} p(r,f|s) \log \frac{p(r,f|s)}{p(r|s)p(f|s)} \\ &= \sum_s p(s) \mathrm{MI}(I_r, I_f^T|s) \ ,\end{aligned} \tag{3}$$

which is equivalent to (1). They also showed that the cMI registration performed better than the registration using the original RMI measure [13].

However, the registration using the sum of local measures to encode spatial information has the disadvantage of being computationally expensive. For example, the cMI registration has been shown to be over ten times slower than the registration using traditional MI measures [13]. The computation becomes

Manuscript received March 22, 2011; accepted April 22, 2011. This work was supported by EPSRC grant EP/H02025X/1. *Asterisk indicates corresponding author.*

*X. Zhuang, S. Arridge, D. J. Hawkes, and S. Ourselin are with Centre for Medical Image Computing, Medical Physics & Bioengineering Department, University College London, The Engineering Front Building, Malet Place, WC1E 6BT, UK (e-mail: x.zhuang@ucl.ac.uk; homepage: http://www.cs.ucl.ac.uk/staff/x.zhuang)

much more expensive when more sample points are used from larger user-defined local regions, which will be illustrated within this article (Section III-C and IV-A). Defining small local regions for its associated spatial variable values, however, could lead to the joint histogram having small number of sampling points, in particular for two dimensional (2D) cases. The entropy measure computed from such joint histogram may lose the statistical power and global intensity class linkage. Hence, the registration may not have robust performance [14]–[16].

Hermosillo *et al.* [9] proposed to associate the PDFs with voxel s to extend the MI registration to the local measures:

$$p_s(r,f) = \frac{1}{\sum \mathcal{W}_s(x)} \sum_{x\in\Omega} \omega_r(I_r(x))\omega_f(I_f^T(x))\mathcal{W}_s(x) \ , \quad (4)$$

which will be shown to be a scheme of encoding spatial information in Section III-A, where $\mathcal{W}_s(x)$ is a weighting function. Klein *et al.* [10] extended the work of [9], [11] and proposed a stochastic optimization scheme where one local measure associated to a random spatial coordinate was computed at each iteration.

In this work, we present a new registration method using spatially encoded mutual information. We first introduce a framework of spatial information encoding, which is achieved by introducing a spatial variable and computing the associated entropy measures according to the spatial coordinates of sample points [7], [8]. We then present an efficient optimization scheme for this nonrigid registration method. Finally, we demonstrate the relation between the proposed registration scheme and the existing works, and explore alternative implementations.

The rest of the paper is organized as follows: Section II provides an insightful interpretation of the problems in nonrigid registration; Section III elaborates on the method; Section IV presents the validation work using four experiments, where discussion is also provided; our conclusions are finally given in Section V.

II. Interpretation of the problems

A. Definition of terms and notations

Intensity distribution: Intensity distribution describes the appearance and contrast of organs presented in a medical image.

Intensity class: It is assumed in this study that the imaged intensity values should be related to the tissue types for the intensity-based registration, meaning n_{tis} intensity values may be presented in an image scanned from n_{tis} types of tissues. However, the intensity of a tissue normally has an intensity range in *in vivo* scans and a number of different tissues, referred to as a class of tissues, may have their intensity ranges overlapping. Therefore, the intensity distribution of the image is presented as n_C classes of intensity ranges, referred to as *intensity classes*. In MI registration where histogram bins are regarded as intensity classes, the intensity range of a tissue may correspond to a number of intensity classes.

Global intensity class linkage: The intensity class correspondence, reflecting the true joint intensity distribution of the two images, is normally unknown before registration due to the misalignments in local regions. By assuming that the two images are initially close to a true match and regarding the local misalignment as noise, we can estimate this correspondence using the approximated joint intensity distribution with sufficient data from global intensity information of the two images [9]. This global information is referred to as *global intensity class linkage*.

Spatial variable s and local region Ω_s: Spatial variable s is an index of a set of spatial coordinates, $s = 1 \dots n_s$. In this work, because we use free-form deformation (FFD) model [17], we define s using the coordinates of control points in the FFD model, similar to the work in [12]. However, it should be noted that the definition of s may be based on user-defined coordinates or randomly selected positions [10], particularly in registration using non-parametric transformation models. It is also common to define a local region Ω_s for s such as the user-defined cubic regions [11] or the local support volume of the FFD control point [12].

SEMI: Spatially encoded mutual information and its registration using local ascent optimization scheme are referred to as SEMI and SEMI registration, respectively.

B. Insight of the problem

One popular interpretation of the MI function is based on dispersion of the joint histogram, meaning that the less dispersed the joint histogram is, the better the two images are assumed to be registered [6]. Under this interpretation, the maximization of MI is related to the minimization of the dispersion of the joint histogram. This interpretation is equivalent to assume an intensity class correspondence between the two images in the MI-based registration.

The advantage of this assumption is the applicability of MI to images with nonlinear relationship of intensity distributions, including images from different imaging modalities where image intensity classes reflect tissue classes. However, MI registration may be inappropriate in certain situations when the optimal alignment is not corresponding to the minimum dispersion of the joint histogram or the assumption of intensity class correspondence.

The first common situation happens in registering *in vivo* medical images with intensity *non-uniformity* (INU), also referred to as intensity *distortion* or intensity *bias*. Fig. 1 shows an example of registering two initially aligned brain MR images [18], where one contains INU while the other does not. The nonrigid registration using NMI measure [4] generates a large erroneous deformation field, shown in Fig. 1 (d). This deformation field also corresponds to the pattern of the INU field map in Fig. 1 (c), meaning the error is not solely caused by the interpolation used in the registration. This is because the joint histogram table is dispersed by the INU compared to the histogram of the two MR images without INU, as Fig. 2 (a) and (b) show. The nonrigid registration using NMI can not further minimize the dispersion of Fig. 2 (a), but can still further *optimize* Fig. 2 (b) to as less dispersed as Fig. 2 (c). This optimization however leads to the registration error shown in Fig. 1 (d).

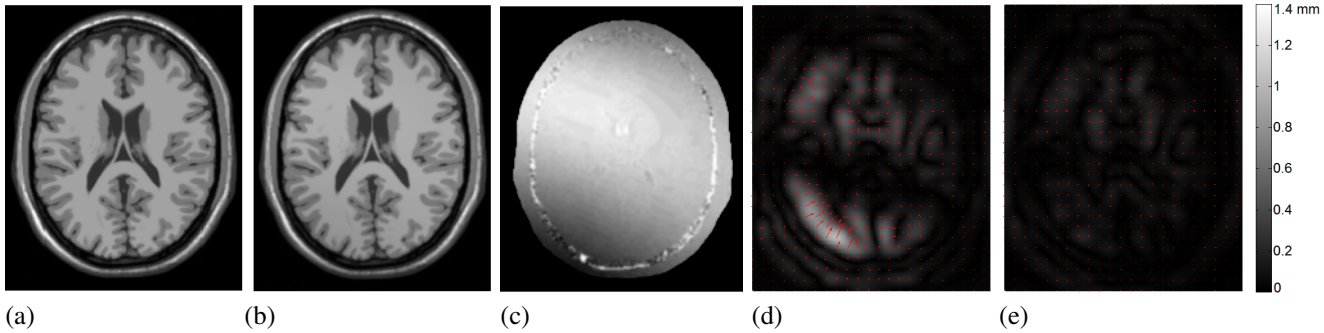

Fig. 1. (a) T1-weighted brain image without intensity non-uniformity (INU) field and (b) the image with INU; (c) the INU field map within the brain. (d) is the resultant deformation field of registering (a) to (b) using normalized mutual information measure and (e) is the deformation field of registering the two images using the proposed registration method. The bar on right indicates the scale of the magnitude of the deformation fields (d) and (e).

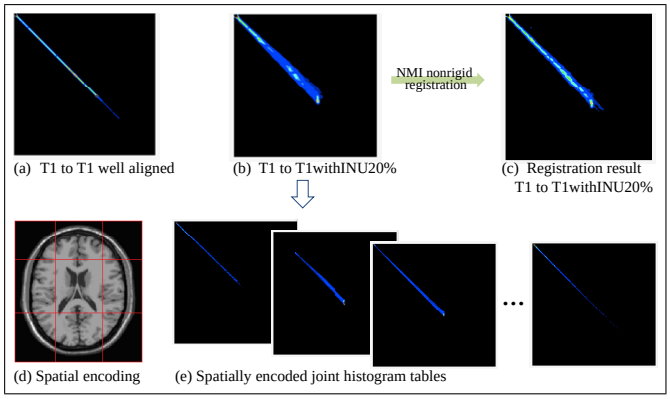

Fig. 2. Illustration of spatial encoding: (a) joint histogram of two T1 brain MR images without INU field; (b) joint histogram of a T1 brain MR image without INU (Fig. 1 (a)) and a T1 brain MR image with a 20% INU field (Fig. 1 (b)); (c) joint histogram of the two images after nonrigid registration using NMI; (d) illustration of dividing an image into a number of local regions; (e) the set of joint histogram tables of the two images on each local region.

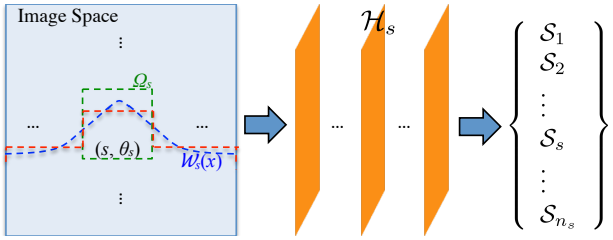

Fig. 3. The spatial variable s and its associated local region Ω_s, transformation parameter θ_s, weighting function $\mathcal{W}_s(x)$, joint histogram $\mathcal{H}_s$, and entropy measure $\mathcal{S}_s$. The spatially encoded similarity measure is the vector representation of $\{\mathcal{S}_s\}$.

The second common situation occurs in registration of contrast enhanced images such as dynamic contrast enhanced MRI [19] or perfusion MRI [20], where the intensity values of images change with respect to the biological uptake of contrast agents.

The third common situation happens in multi-modality registration. For example, in the CT-MR registration application demonstrated in [12], [13], there is one intensity class for several tissue types in CT images. However, the intensity of these tissue types may be represented as a number of intensity classes in MR images.

To interpret the problems, we use dispersion of the joint histogram of the registration images. If we discriminate the spatial difference by dividing the space into several local regions, as Fig. 2 (d) shows, the effect of INU can then be minimized, as the local joint histogram tables in Fig. 2 (e) are less dispersed and unlikely to be further minimized. Based on this idea, we develop a registration scheme to incorporate this spatial information. The registration result in Fig. 1 (e) shows that this method demonstrates a good robustness against the INU field and performs much better compared to NMI registration.

Finally, it is inappropriate to use intensity-based MI registration when one or both of the registration images come from an imaging modality where the imaged pixel intensity values do not represent tissue types. One example is the ultrasound imaging, where the intensity values are related to tissue boundaries and incident angles of the ultrasound beams, instead of directly to the types of homogeneous tissues. In this situation, the intensity class correspondence can not be assumed to be the same correspondence of tissue types between the two images. Hence registration based on features is recommended such as the phase registration [21]. These situations are not considered in this study.

III. Method

We propose to include the spatial information into the nonrigid registration using information theoretic measure to deal with the problems. This is achieved by introducing a spatial variable s and computing its associated joint histogram $\{\mathcal{H}_s\}$. The contribution of pixels to the computation of $\mathcal{H}_s$ is varied according to their spatial coordinates. A set of entropy measures $\{\mathcal{S}_s\}$ are then computed from $\{\mathcal{H}_s\}$, as illustrated in Fig. 3.

A. The framework of spatial information encoding

To compute $\mathcal{S}_s$, we can estimate the associated joint histogram $\mathcal{H}_s$ using the information solely within the associated local region Ω_s, referred to as *local information*, as follows:

$$\mathcal{H}_s(r, f) = \sum_{x \in \Omega_s} \omega_r(I_r(x))\omega_f(I_f^T(x)) \ , \qquad (5)$$

For $\mathcal{H}_s(r, f)$, the weights of all pixel $x \in \Omega_s$ are equal to one, and the weights of pixel $x \notin \Omega_s$ are all zero, regardless

of their different spatial coordinates. This weighting scheme is illustrated as the red dash-line in Fig. 3 (left).

In this work, we propose a weighting scheme such that the weight of pixels is monotonically decreasing with respect to the distance between x and the coordinate of s for $\mathcal{H}_s(r,f)$. This weighting function is illustrated as the blue dash-line in Fig. 3 (left). The joint histogram $\mathcal{H}_s(r,f)$ is then given by:

$$\mathcal{H}_s(r,f) = \sum_{x\in\Omega} \omega_r(I_r(x))\omega_f(I_f^T(x))\mathcal{W}_s(x) \ , \qquad (6)$$

where $\mathcal{W}_s(x)$ is the weighting function for spatial information encoding. Accordingly, the joint PDF is given by: $p_s(r,f) = \frac{1}{N_s}\mathcal{H}_s(r,f)$, where $N_s = \sum_{r,f}\mathcal{H}_s(r,f)$ is the normalization factor.

The derivative of $\mathcal{H}_s(r,f)$ with respect to a transformation parameter θ_t is given by:

$$\frac{\partial\mathcal{H}_s(r,f)}{\partial\theta_t} = \sum_{x\in V_t} \frac{\partial\omega_f(I_f^T(x))}{\partial\theta_t}\omega_r(I_r(x))\mathcal{W}_s(x) \ , \qquad (7)$$

where V_t *is the local support volume* of the transformation parameter θ_t. The computation of $\partial\omega_f(I_f^T(x))/\partial\theta_t$ is the same as that in the traditional MI registration [1]–[3]. The computation complexity of (7) is $O(|\Omega_s \cap V_t|)$, because the update for the joint histogram table is only within the local support volume of θ_t and the local region of $\mathcal{W}_s(x)$. The computation for marginal histogram $\mathcal{H}_s(r)$ and $\mathcal{H}_s(f)$ is similar. Based on this, MI or the normalized measures and their derivatives can be computed.

Given the transformation is a FFD model, $T(x) = x + \sum_{ijk}\mathcal{B}_{ijk}(x)\theta_{ijk}$, then (7) becomes:

$$\frac{\partial\mathcal{H}_s(r,f)}{\partial\theta_t} = \sum_{x\in V_t} \omega'_f(a)(\nabla I_f(y)\mathcal{B}_t(x))\omega_r(I_r(x))\mathcal{W}_s(x) \ , \qquad (8)$$

where $\mathcal{B}$ is cubic B-spline kernel function, $a = I_f(y)$ and $y = T(x)$.

B. Choices of $\mathcal{W}_s(x)$ and regularization of locality using hierarchy scheme

In this study, we use the Gaussian kernel function for $\mathcal{W}_s(x)$:

$$\mathcal{W}_s(x) = Ae^{-\left(\frac{(x_1-\phi_{s1})^2}{2\sigma_1^2}+\frac{(x_2-\phi_{s2})^2}{2\sigma_2^2}+\frac{(x_3-\phi_{s3})^2}{2\sigma_3^2}\right)} \ , \qquad (9)$$

where $A = 1$ and $[\sigma_1,\sigma_2,\sigma_3]$ are the standard deviations. In practice, we use $\sigma_i = \sigma$ and set the locality of the Gaussian function, Ω_s, to the volume within three times the standard deviation. Hence, the size of the local region is denoted as the spheric diameter $l = 6\sigma$. It should be noted that the computation complexity of the optimization using (16) is not significantly increased along with the increased value of l in FFD registration. This is because the computation is determined by the size of local support volume of the transformation parameter as (7) shows.

The amount of information used in the computation of $\mathcal{H}_s$ in (6) is related to Ω_s, the local region of the weighting function. The more information used in the computation of $\{\mathcal{H}_s\}$, the better statistical power of the computed $\mathcal{S}_s$ and better maintenance of the global intensity class linkage, both of which contribute to better registration robustness. However, the more locality of $\mathcal{W}_s(x)$, the more locality of $\mathcal{S}_s$, and hence the better accuracy in local region Ω_s. A strategy to maintain both of the two advantages is to use a hierarchy scheme by starting the registration using a weighting function with a large local region. Then, we hierarchically change $\mathcal{W}_s(x)$ to functions with smaller local regions. In [12], the hierarchy scheme was implicitly applied by setting the local region to the local support volume of the corresponding control point in the multi-level FFD registration [22]; while in [11], the size of local regions was user-defined. In this work, the local region size is also user-defined and the hierarchy scheme of spatial encoding may not be related to the multi-level FFDs. For example, we could first set the local region diameter l to a value at the top level. Then, at each subsequent level of spatial encoding, l is halved regardless the settings of FFDs.

C. Spatially encoded mutual information

Similarity measure*:* The entropy measures $\{\mathcal{S}_s\}$ are computed from their associated PDFs. This computation results in a vector measure composed of $\{\mathcal{S}_s\}$ between two registration images, as Fig. 3 shows. This measure is referred to as the *spatially encoded mutual information* (SEMI):

$$\text{SEMI} = \{\mathcal{S}_1,\mathcal{S}_2,\cdots,\mathcal{S}_s,\cdots,\mathcal{S}_{n_s}\}^{\mathrm{T}} \ , \qquad (10)$$

To present a scalar value of SEMI, one scheme is to compute the weighted sum of $\{\mathcal{S}_s\}$:

$$\text{SEMI}_{\text{sum}} = \sum_s p(s)\mathcal{S}_s \ , \qquad (11)$$

where $p(s) = N_s/\sum_t(N_t)$.

Alternatively, since SEMI is a vector, the squared magnitude of the vector can be computed as a scalar similarity measure:

$$\text{SEMI}_{\text{mag}} = \sum_s \left(\mathcal{S}_s\right)^2 \ . \qquad (12)$$

The entropy measure $\mathcal{S}_s$ can be the joint entropy, MI, or the normalized forms such as NMI [4] and entropy correlation coefficient [2]. Studholme et al. [4] showed that NMI was robust to the changes in overlap volumes. Therefore, we use NMI for the implementation of $\mathcal{S}_s$ in this work. Notice that the results using other MI forms may not be significantly different.

Driving forces and optimization of SEMI*:* The spatial variable s is defined according to the nonrigid transformation model used in the registration. In this work, we employ the FFD model [5]. The value of s is then defined to the index of the FFD control point θ_t, and Ω_t is the local support volume.

Given the transformation parameter θ_t, the steepest ascent direction of registration using the scalar SEMI is given by the derivative of SEMI in (11) or (12) as follows:

$$\vec{F}_{SA}(\theta_t) \equiv \frac{\partial\text{SEMI}}{\partial\theta_t} = \sum_s \frac{\partial C(\mathcal{S}_s)}{\partial\theta_t}, \quad \text{where } C(\mathcal{S}_s) \text{ refers to (11) and (12)} \ . \qquad (13)$$

The computation complexity of (13) is $O(n|\Omega_s \cap V_t|)$, where n is the number of spatial variable values whose associated joint histogram needs updating. However, this computation may be practically too expensive when n is large, compared to only $O(|V_t|)$ in traditional MI registration.

Since SEMI is a vector of $\{\mathcal{S}_s\}$, the derivative of SEMI vector against θ_t is then given by:

$$\vec{F}(\theta_t) \equiv \{\partial\mathcal{S}_1/\partial\theta_t, \partial\mathcal{S}_2/\partial\theta_t, \ldots, \partial\mathcal{S}_{N_s}/\partial\theta_t\}^{\mathrm{T}} \ . \quad (14)$$

Each $\partial\mathcal{S}_i/\partial\theta_t$ is computed using the result of (8), where when $t \neq s$,

$$\sum_{x\in V_s} \mathcal{B}_t(x)\mathcal{W}_t(x) << \sum_{x\in V_s} \mathcal{B}_s(x)\mathcal{W}_s(x) \ . \quad (15)$$

Therefore, we propose to optimize each $\mathcal{S}_s$ with respect to the associated transformation parameter, the FFD control point θ_s, using a direction of local ascent, ignoring the effects from $\{\partial\mathcal{S}_s/\partial\theta_t\}|_{t\neq s}$:

$$\vec{F}_{LA}(\theta_s) \equiv \partial\mathcal{S}_s/\partial\theta_s \ . \quad (16)$$

The computation complexity of (16) is now *significantly reduced* to $O(|\Omega_s \cap V_s|)$, which compares with $O(n|\Omega_s \cap V_t|)$ of (13) and (14).

Local ascent optimization *uses (16) as the derivative of each transformation parameter and updates all transformation parameters in each iteration as in gradient ascent optimization.* We assume that the optimization of each $\mathcal{S}_s$ should not deteriorate that of others due to the minor effects, and thus should globally converge. The convergence of local ascent optimization for SEMI registration will be validated in Section IV-A. The comparisons with the registration of $\mathrm{SEMI}_{\mathrm{sum}}$, $\mathrm{SEMI}_{\mathrm{mag}}$, and NMI using global ascent optimization will also be provided.

Klein *et al.* [10] proposed a stochastic optimization scheme for the registration using sum of $\{\mathcal{S}_s\}$. In their work, they used one value of s associated to a randomly selected spatial coordinate in each iteration, and optimized the single corresponding local measure in this step. The computation complexity in each iteration was similar to that in traditional MI registration. Without considering the randomness of s value, Klein's scheme is similar to optimizing one individual local measure of $\{\mathcal{S}_s\}$ in each iteration.

The implementation of gradient ascent optimization in this work uses decreasing step length, without line-search, to advance in each iteration [16]. The optimization is stopped when the similarity measure can not be further improved within the last five steps or when the optimization reaches the number of user-defined maximal iteration steps.

D. Relation to existing work

Spatial information encoding is determined by the weighting scheme in $\mathcal{W}_s(x)$. By using a constant value such that $\mathcal{W}_s(x) = 1$, the computed measure $\mathcal{S}_s$ is identical to traditional entropy measures such as the global MI or NMI.

In [7], the spatially encoded PDF $p_s(r, f)$ was given by a mixture model:

$$p_s(r, f) = (1 - w)p_{_L} + wp_{_G} \ , \quad (17)$$

where $p_{_L} = \frac{1}{N_{_L}} \sum_{x\in\Omega_{_L}} \omega(\circ)$ is estimated from a subvolume $\Omega_{_L}$ and $p_{_G} = \frac{1}{N_{_G}} \sum_{x\in\overline{\Omega}_{_L}} \omega(\circ)$ is estimated from the complementary volume $\overline{\Omega}_{_L}$; $\omega(\circ) = \omega_r(I_r(x))\omega_f(I_f^T(x))$ and $N_{_L}$ and $N_{_G}$ are the normalization factors. The equation (17) can be rewritten as follows:

$$p_s(r, f) = \frac{1}{N} \sum_{x\in\Omega_{_L}} \omega(\circ)\frac{(1-w)N}{N_{_L}} + \frac{1}{N} \sum_{x\in\overline{\Omega}_{_L}} \omega(\circ)\frac{wN}{N_{_G}} \ , \quad (18)$$

where $N = N_{_L} + N_{_G}$. This spatial information encoding scheme is equivalent to using two constant values for weighting function $\mathcal{W}_s(x)$:

$$\mathcal{W}_s(x) = \begin{cases} \frac{(1-w)N}{N_{_L}}, & x \in \Omega_{_L} \\ \frac{wN}{N_{_G}}, & x \in \overline{\Omega}_{_L} \end{cases} \ . \quad (19)$$

Using the cubic B-spline fuction β^3 we have

$$\mathcal{W}_s(x) = \beta^3_{\Delta_1}(x_1 - \phi_{s1})\beta^3_{\Delta_2}(x_2 - \phi_{s2})\beta^3_{\Delta_3}(x_3 - \phi_{s3}) \ , \quad (20)$$

where $x = [x_1, x_2, x_3]^{\mathrm{T}}$ is the coordinate of the pixel x, $[\phi_{s1}, \phi_{s2}, \phi_{s3}]^{\mathrm{T}}$ is the coordinate of the s corresponded FFD control point, and $[\Delta_1, \Delta_2, \Delta_3]$ are the FFD spacings in each dimension. Then, $\mathcal{H}_s$ turns to be the 3D joint histogram $\mathcal{H}(r, f, s)$ in [12] and $p_s(r, f)$ becomes the conditional PDF $p(r, f|s)$. The corresponding $\mathrm{SEMI}_{\mathrm{sum}}$ is then given by:

$$\mathrm{SEMI}_{\mathrm{sum}}|_{\mathcal{S}_s=\mathrm{MI}} = \sum_s p(s) \sum_{r,f} p(r, f|s) \log \frac{p(r, f|s)}{p(r|s)p(f|s)} \ , \quad (21)$$

which is the cMI in [12]. By using the *boxcar* function for $\mathcal{W}_s(x)$, (21) becomes the RMI′ measure, (1), derived in [11].

IV. Experiments and results

This section consists of five experiments to validate the proposed SEMI registration method. Section IV-A validates the local ascent optimization of SEMI, and Section IV-B shows the difference of using different weighting schemes in SEMI registration. Section IV-C investigates the performance of SEMI and NMI registration in different magnitudes of INU fields. Section IV-D and IV-E shows the application of SEMI to the registration of dynamic contrast enhanced MRI of the liver and *in vivo* cardiac MR images, where comparisons with NMI registration are also provided.

In Section IV-C, IV-D and IV-E, SEMI registration used the Gaussian kernel function for spatial information encoding and the hierarchy scheme for locality regularization. In all the experiments in this work, the multi-level FFD scheme [22] and the concatenation of a series of isotropic FFDs [23] were employed for the transformation modeling; the multiresolution scheme [24] were adopted in the optimization and 64 bins were used for joint histogram table construction.

A. Local ascent optimization

Data and experimental setup: This experiment used 2D brain MR T1 images to study the validity of local ascent optimization. The images were downloaded from BrainWeb [18], with image size $181 \times 217 \times 181$ and voxel size $1 \times 1 \times 1$ mm.

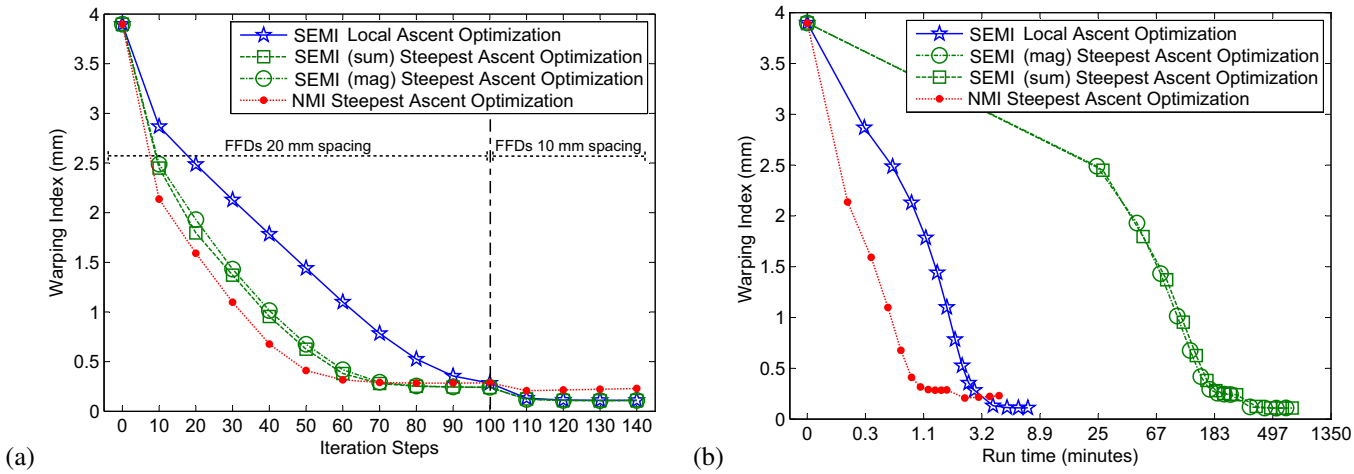

Fig. 4. (a) The mean registration errors, warping index, of the four methods in every 10 iteration steps. (b) Warping index against the run time (the scale is logarithmic) plot.

We only selected the middle slice from the axial view for this experiment. One of the registration images did not have INU while the other had a 20% INU field. The initial transformations, regarded as the ground truth for the registration accuracy assessment, were combinations of isotropic scaling and FFD transformations [5] with 45×54 mm mesh spacing. The scaling values were chosen from (0.9, 1.1) and the FFD transformations moved the central control points either 15 mm or -15 mm at each direction. Warping index, root mean square (RMS) residual displacement errors, was calculated as the registration accuracy. The accuracy was assessed within the brain. It should be noted that the purpose of this experiment was to compare the computation time of different registration schemes. Hence, the simulated deformation fields were not specifically designed to be representative of real deformations occurred in registration of brain images. Similar simulation methods were also used in the next two brain image registration experiments (Section IV-B and IV-C), where the difference of registration accuracy using different spatial encoding schemes and INU levels was studied.

We generated 24 initial deformation fields to deform the floating image. Two level FFD meshes, isotropic 20 mm and isotropic 10 mm, were used for all registration tasks where 100 iteration steps were first employed for the 20 mm FFD level, and then 40 steps for the 10 mm FFD level.

The steepest ascent optimization, of (13), was applied to SEMI using sum of $\{\mathcal{S}_s\}$, to SEMI using magnitude of $\{\mathcal{S}_s\}$, and to NMI registration, referred to as $\text{SEMI}^{\text{SA}}_{\text{sum}}$, $\text{SEMI}^{\text{SA}}_{\text{mag}}$, and NMI respectively. The SEMI registration using the local ascent optimization, (16), is referred to as SEMI. The Gaussian function encoding and hierarchy scheme was used.

Results and discussion: Fig. 4 (a) illustrates the mean registration errors (warping index) by the four methods. They are displayed in every 10 iteration steps. The mean warping index is also displayed in Table I where the small standard deviation values, less than 0.01 mm, indicate that all of the four registration schemes performed consistently in the test cases. Table I also shows that NMI registration needed the least computation time, but its mean warping index was larger than the other three registration schemes.

For the SEMI registration schemes, the computation of each iteration step in SEMI was more than 100 times faster than those of $\text{SEMI}^{\text{SA}}_{\text{sum}}$ and $\text{SEMI}^{\text{SA}}_{\text{mag}}$, as Table I shows. The local ascent optimization of SEMI needed more iterations steps to converge than $\text{SEMI}^{\text{SA}}_{\text{sum}}$ and $\text{SEMI}^{\text{SA}}_{\text{mag}}$ (Fig. 4 (a)) did. However, the computation time was much less, as the plot of the warping indices against run time in Fig. 4 (b) shows. Furthermore, there was no statistically significant difference in terms of registration accuracy between the use of the local ascent optimization and that of the two global steepest ascent schemes, as the p-value of the two tailed, paired t-test between SEMI and $\text{SEMI}^{\text{SA}}_{\text{sum}}$ was 0.462, and that between SEMI and $\text{SEMI}^{\text{SA}}_{\text{mag}}$ was 0.662. In practice, one may consider to use NMI registration, which is fast and equivalent to the SEMI registration with $\mathcal{W}_s(x) = 1$, for initialization and then use the proposed SEMI, which can achieve high accuracy, for refinement. Finally, as this experiment used 2D images, one may have different results using original 3D images. However, the conclusion is expected to be the same and the run time difference can be more significant in 3D cases.

B. *Different spatial encoding schemes*

Data and experimental setup: This experiment used 3D brain MR T1 images, downloaded from BrainWeb, to demonstrate SEMI registration using different spatial information encoding schemes. One of the registration images did not have INU while the other had a 20% INU field. Sixty initial transformations, regarded as ground truth for the registration accuracy assessment, were generated using the similar method described in the previous experiment in Section IV-A. Ten registration schemes were used to recover the deformation fields, including NMI registration, four SEMI registration schemes using the mixture model for spatial encoding, and five SEMI registration schemes using the Gaussian function for spatial encoding. All of the ten registration methods used three level FFD meshes, isotropic 40 mm, isotropic 20 mm, and isotropic 10 mm, as the transformation model.

TABLE I
THE REGISTRATION ACCURACY, GIVEN BY WARPING INDEX (WI), OF THE FOUR REGISTRATION SCHEMES. THE TABLE ALSO GIVES THE RATIOS OF COMPUTATION TIME (RCT) OF THE OTHER THREE METHODS TO THAT OF THE SEMI, AND THE P-VALUES BETWEEN THE REGISTRATION ACCURACY OF SEMI AND THAT OF THE OTHER THREE METHODS.

	NMI	$\text{SEMI}^{\text{SA}}_{\text{sum}}$	$\text{SEMI}^{\text{SA}}_{\text{mag}}$	SEMI
WI (0.01 mm)	23 ± 0.9	11 ± 0.6	11 ± 0.5	11 ± 0.7
RCT	0.60	160	144	1
P-value	$<$0.0001	0.462	0.662	—

TABLE II
WARPING INDICES (MM) OF THE TEN REGISTRATION METHODS.

NMI	mx.75	mx.5	mx.25	mx0
$.414 \pm .017$	$.332 \pm .042$	$.310 \pm .044$	$.302 \pm .043$	$.301 \pm .052$
gau200	gau100	gau50	gau25	gaumul
$.176 \pm .016$	$.099 \pm .016$	$.155 \pm .160$	$.877 \pm 1.08$	**$.085 \pm .012$**
bsp200	bsp100	bsp50	bsp25	bspmul
$.152 \pm .017$	$.091 \pm .014$	$.173 \pm .214$	1.40 ± 1.59	**$.082 \pm .010$**

In the mixture model encoding scheme (18), we used w=0.75 (denoted as mx.75), w=0.5 (denoted as mx.5), w=0.25 (denoted as mx.25), and w=0 (denoted as mx0), respectively. This category of methods are referred to as {mx}. In {mx}, the local regions, Ω_L in (18), were set to the local support volumes of control points. Hence, the locality of registration mx0 was a three-level hierarchy scheme, from 160 mm, 80 mm, to 40 mm. For all the other methods in {mx}, the locality was the whole image.

In the Gaussian function weighting scheme (9), we used l=200 mm for the size of local regions (denoted as gau200), l=100 mm (denoted as gau100), l=50 mm (denoted as gau50), l=25 mm (denoted as gau25), and the scheme where the size of local regions hierarchically deceased from l=200 mm to 25 mm (denoted as gaumul), respectively. This category of methods are referred to as {gau}. Similarly, the methods using the cubic B-spline kernel function weighting scheme and same settings of l as in {gau} are denoted and referred to as {bsp}.

Results and discussion: Fig. 5 plots the Box-and-Whisker diagrams of the registration results, warping indices, by the ten registration methods, and Table II presents the mean and standard deviation of them. The results show that NMI and all {mx} SEMI registrations achieved good registration robustness, but the accuracy was limited. The {mx} registration could provide better accuracy than NMI registration. However, the improvement was not as significant as {gau} or {bsp}. For example, registration mx0 achieved larger mean warping index compared to gau200 and gau100, both of which used larger local region size (less locality) compared to that of mx0 (40mm). Also, neither gau200 nor gau100 used hierarchy scheme.

Within {gau}, the results showed that the registration had the potential to achieve better registration accuracy, when the local measure was assigned with more locality (assigning l with smaller values). However, the locality could also lead to reduced robustness, as the results of gau50 and gau25 show. Finally, the SEMI registration with the hierarchy scheme (gaumul) achieved both good accuracy (mean warping index: 0.085 mm) and robustness (standard deviation: 0.012 mm). Similar

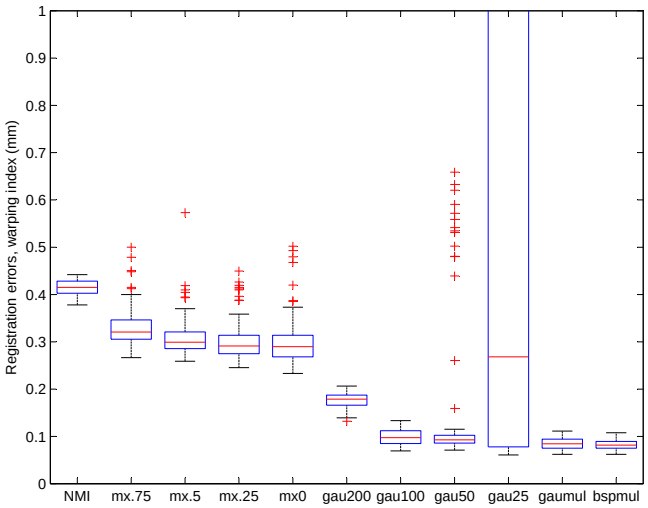

Fig. 5. Box-and-Whisker plots of the registration results using NMI and SEMI registration with different encoding schemes. The encoding schemes include the mixture model with w=0.75 (mx.75), w=0.5 (mx.5), w=0.25 (mx.25), w=0 (mx0), and the Gaussian kernel function weighting scheme with local region size l=200 mm (gau200), l=100 mm (gau100), l=50 mm (gau50), l=25 mm (gau25), and hierarchy scheme from l=200 mm to l=25 mm (gaumul) and the same hierarchy scheme using BSpline kernel function (bspmul). Note that some cases from gau50 and gau25, whose warping indices are more than 1 mm, are not displayed here.

conclusion can be drawn within {bsp}, as results in Table II shows. Compared to {gau}, cubic B-spline demonstrated more locality when the local region size was set to the same as {gau}. For example, the accuracy of bsp200 and bsp100 was better than that of gau200 and gau100, while the robustness of bsp50 and bsp25 was worse than that of gau50 and gau25. However, the difference of the two schemes was much smaller when the hierarchy scheme was used, as the warping indices of gaumul and bspmul were 0.085 ± 0.012 and 0.082 ± 0.010 (mm) respectively and the box-and-Whisker plots of them, shown in Fig. 5, also look similar.

C. Performance to intensity non-uniformity

Data and experimental setup: This experiment employed 3D brain MR images to study the performance of NMI and SEMI registration in different magnitudes of INU fields. The MR images, with 3% noise fields, were downloaded from the BrainWeb. We generated eleven INU fields from 0% to 20%. We then used forty-eight initial deformations for each level of INU fields. These deformations were generated using the same method used in Section IV-B. Both the SEMI and NMI registration used three level isotropic FFDs (40 mm, 20 mm and 10 mm) and SEMI was the hierarchy scheme (gaumul) in the previous section. Warping index within the brain was computed as the registration accuracy.

Results and discussion: Fig. 6 plots the Box-and-Whisker diagrams of the 48-case results by NMI and SEMI registration in different magnitudes of INU fields, and Table III presents the mean and standard deviation of the warping indices. The results show that NMI achieved no worse registration accuracy in the registration of none-INU (0%) cases. However, in the cases of images with INU, the warping indices of NMI

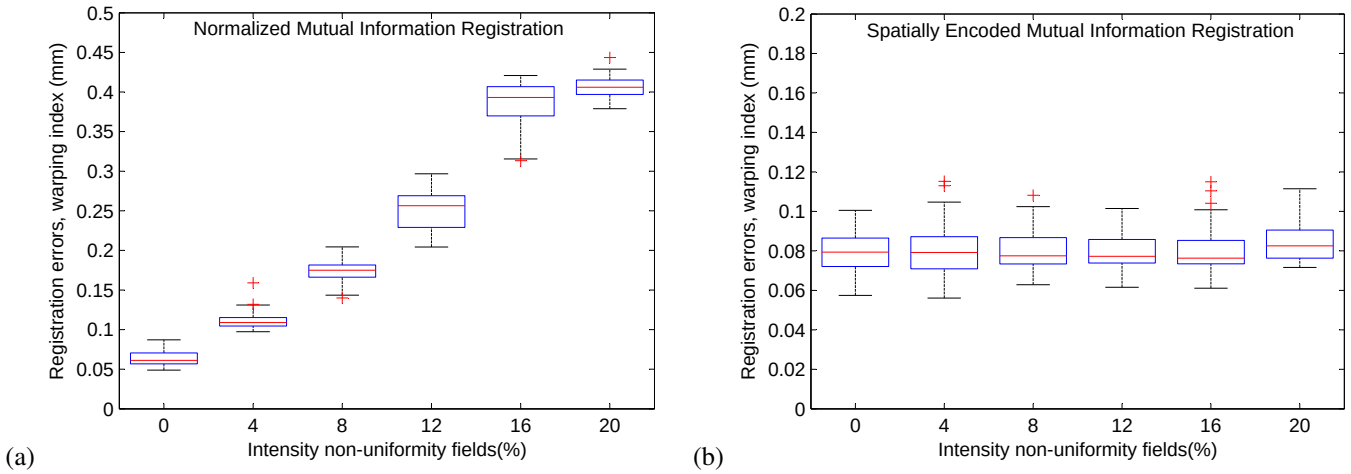

Fig. 6. The Box-and-Whisker diagrams of 48-case registration errors by SEMI (a) and NMI registration (b) in different intensity non-uniformity fields.

TABLE III
WARPING INDICES (MM) OF NMI AND SEMI REGISTRATION IN DIFFERENT MAGNITUDE OF INTENSITY NON-UNIFORMITY FIELDS.

(mm)	0%	4%	8%	12%	16%	20%
NMI	$.063 \pm .009$	$.111 \pm .011$	$.174 \pm .015$	$.251 \pm .026$	$.385 \pm .029$	$\mathbf{.407 \pm .014}$
SEMI	$.080 \pm .011$	$.081 \pm .013$	$.080 \pm .010$	$.080 \pm .009$	$.080 \pm .011$	$\mathbf{.085 \pm .010}$

registration were bigger than that of SEMI registration. Also, the performance difference between the two methods became more evident when the INU field became stronger. Fig. 6 (b) and Table III also show that SEMI registration performed fairly consistently with respect to different levels of INU, as the mean and median warping indices were all around 0.08 mm. However, NMI registration had radically increased warping indices when the INU fields became stronger.

D. Application to dynamic contrast enhanced MRI

Data and experimental setup: This experiment employed four sets of simulated dynamic contrast enhanced (DCE) MRI data of the liver. DCE MRI causes time-varying intensity values and consequently changes the tissue and intensity class correspondence between images from different time points [19], [25]. Fig. 7 shows an example whose registration results are plotted in Fig. 8 (c).

The DCE MRI data had simulated free-breathing motions which deformed the images. The four sets of DCE MRI data were with different magnitudes of motions. Nonrigid NMI and SEMI registration was applied to recover the respiratory motions respectively. The transformation was the FFD transformation model [5]. SEMI registration used two level hierarchy scheme (gaumul), starting with 80 mm for the local region size at the top level. The images from different time points were all registered to the reference image, the MR image without enhancement, to correct the deformations in the liver. The warping index was calculated on the liver region which was the interest of the registration.

Results and discussion: Fig. 8 plots the mean warping index by the two registration methods. SEMI registration performed better than NMI registration, particularly during the time points between 5 to 10 when the contrast agent started to enter the liver region and changed the intensity values. The results also show that during the time points 1 to 5, SEMI registration did not achieve evidently better mean warping index than NMI registration. This was because the intensity of the liver region had not been changed in these time points, as the contrast agent had not yet arrived. From time point 10 to 15, the contrast agent in the liver was in late enhancement and the intensity distributions were more uniform. Therefore, NMI registration achieved better registration results, but the warping indices were still not as good as these of SEMI registration because there was still INU remained in the images due to the enhancement.

E. Application to clinical cardiac MR registration

Data and experimental setup: This experiment employed a set of twenty clinical cardiac MR volume, scanned from twenty different subjects using an isotropic, volumetric MR sequence which images the heart on the end-diastolic phase [26]. For each MR image, the surfaces of the substructures have been manually delineated, including the endocardium of the four chambers and the epicardium of the left ventricle. Fig. 9 shows one example of an MR image (a) and its manually delineated surfaces (b).

These MR images contained noise, artifacts, and INU due to the variation of scanning environments, the parameters of the MRI sequence, and the varying physiological conditions of the subjects. Therefore, we employed this experiment to test whether the SEMI registration, with the encoding of spatial information, was able to achieve a better registration accuracy compared to the NMI registration. In the experiment, SEMI registration used two level hierarchy scheme (gaumul), starting with 80 mm for the local region size at the top level.

The experiment was designed as follows: every image from this data pool was considered as a reference image and registered to one floating image "randomly" selected from

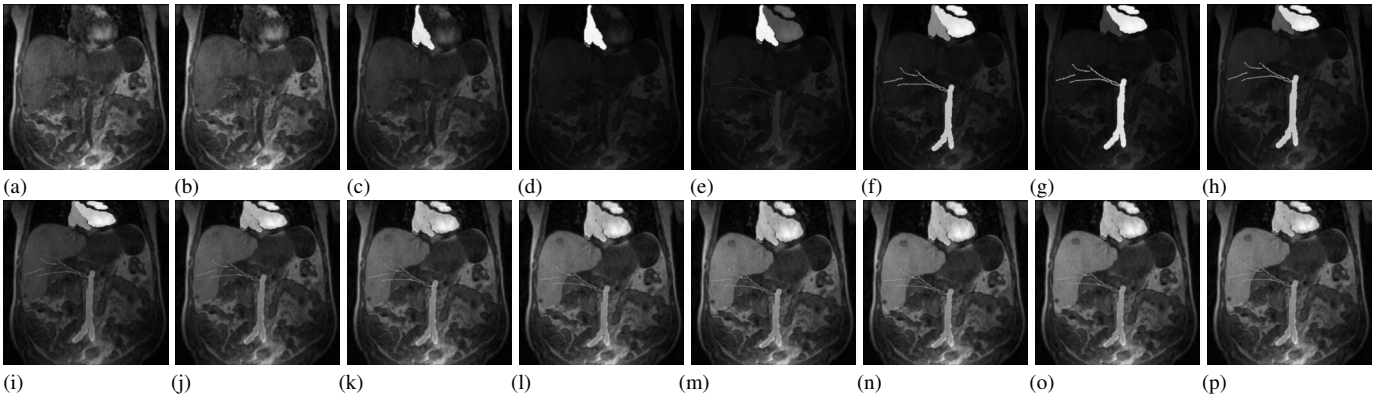

Fig. 7. One example of the simulated dynamic contrast enhanced MR data in fifteen time points. Image (a) is the reference image without contrast enhancement. Images (b)-(p) are the dynamic enhanced data from time point one to fifteen.

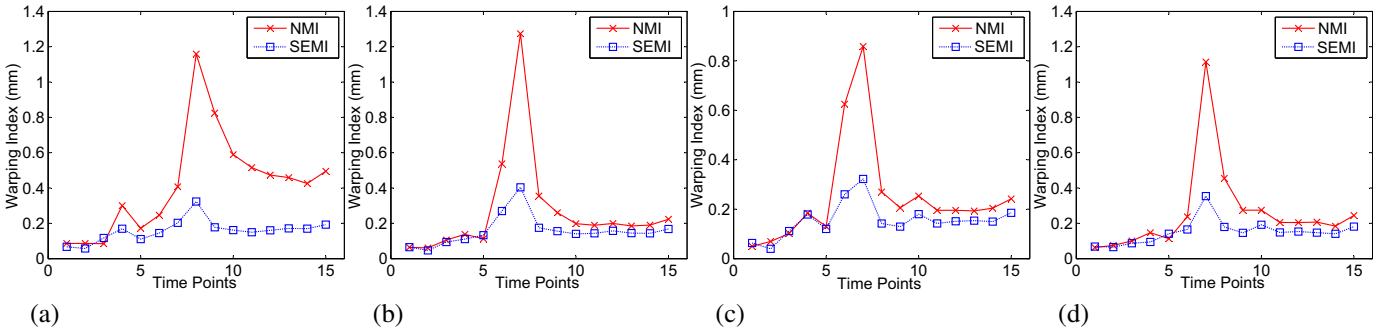

Fig. 8. Registration accuracy of the four simulated dynamic contrast enhancement MRI cases by normalized mutual information (NMI) and spatially encoded mutual information (SEMI) .

TABLE IV
THE ERRORS OF NMI AND SEMI REGISTRATION ARE ASSESSED USING THE ROOT MEAN SQUARE (RMS) SURFACE DISTANCE BETWEEN THE SURFACES OF THE TWO REGISTERED IMAGES. THE TABLE ALSO GIVES THE P-VALUE AND 95% CONFIDENCE INTERVAL (CI) OF THE TWO TAILED, PAIRED T-TEST BETWEEN THE TWO GROUPS OF REGISTRATION RESULTS.

NMI error (mm)	SEMI error (mm)	P-value [CI (mm)]
1.56 ± 0.55	1.19 ± 0.21	0.0005 [0.192, 0.563]

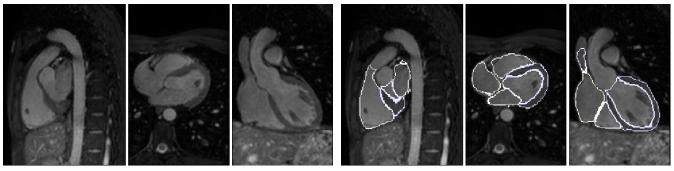

Fig. 9. Example of an MR image (a) and its manually delineated surfaces (b). Images shown in sagittal, axial, and coronal views.

the rest of the data pool. The "randomly" is quoted because the selection of floating images was deliberately designed to avoid a repeated registration combination by swapping the reference and floating images. This selection hence presented 20 different registration tasks as a test set. We initialized the substructures of the heart for all the registration cases using the locally affine registration method [27], [28]. Then, the nonrigid registration of NMI or SEMI was applied to fine-tune the local details. The nonrigid transformation model was again the FFDs, and the registration errors were calculated from the RMS surface distance between the four chamber surfaces of the reference image and the deformed floating image.

Results and discussion: Table IV presents the RMS surface distance error of the two registration schemes. The mean error of SEMI registration was significantly improved compared to that of NMI registration: the difference of them was 0.37 mm (P=0.0005, 95% confidence interval [0.192, 0.563] mm). This difference also indicated that there were INU and artifacts in the MR images, which resulted in larger surface distance errors for the nonrigid NMI registration.

V. CONCLUSION

In this work, we have investigated the registration using information theoretic measures, such as the normalized mutual information (NMI), and the limitation when applied to non-rigid registration. We presented a framework to encode spatial information in the computation of a spatial variable and its associated entropy measures. This encoding is achieved by using a weighting scheme to differentiate the contribution of sample points to the different joint histogram tables which are associated with different spatial variable values. A hierarchy scheme is also used to regularize the locality of the weighting function. We then developed a nonrigid registration framework for spatially encoded mutual information (SEMI), where the nonrigid transformation is modeled by the free-form deformations (FFDs) and the spatial variable is defined to the coordinates of FFD control points. The similarity in this SEMI registration consists of a set of entropy measures and has a vectorial representation. To efficiently search the optimum, we

proposed the local ascent optimization scheme, where the local support effect of control points in FFD registration is utilized for fast computation of driving forces.

We validated our proposals using five experiments where brain MR, dynamic contrast enhanced MRI (DCE MRI) of the liver, and clinical cardiac MR data were used. The experiment in Section IV-A demonstrated the convergence of the local ascent optimization, which achieved similar accuracy as the scheme of global steepest ascent optimization using the two scalar representation of SEMI. However, the proposed SEMI registration saved over 100 times computation time in each iteration. Section IV-B showed that it is important to use the hierarchy scheme to regularize the locality of the spatial information encoding, in order to maintain the registration robustness and achieve high accuracy.

The experiment in Section IV-C investigated the performance of SEMI and NMI registration in images with different magnitudes of intensity non-uniformity. It has been shown that SEMI performed better when the images were with intensity non-uniformity, and the superiority of SEMI was more evident when the intensity non-uniformity became stronger. We further applied SEMI and NMI to the registration of DCE MRI of the liver and clinical cardiac MR data in Section IV-D and IV-E. Compared to NMI registration, SEMI registration performed better from the time point when the contrast agent flushed in the DCE MRI application, and it significantly improved the registration accuracy in the cardiac MR application.

ACKNOWLEDGMENT

The authors would like to thank colleagues Dr. Andrew Melbourne and Dr. David Atkinson, and Dr. David Collins from Institute of Cancer Research, Royal Cancer Hospital, London for providing the DCE MRI simulation tool and data.

REFERENCES

[1] P. Viola and V. M. Wells, III, "Alignment by maximization of mutual information," *International Journal of Computer Vision*, vol. 24, no. 2, pp. 137–154, 1997.

[2] F. Maes, A. Collignon, D. Vandermeulen, G. Marchal, and P. Suetens, "Multimodality image registration by maximization of mutual information," *IEEE Transactions of Medical Imaging*, vol. 16, no. 2, pp. 187–198, Apr. 1997.

[3] W. M. Wells III, P. Viola, H. Atsumi, S. Nakajima, and R. Kikinis, "Multi-modal volume registration by maximisation of mutual information," *Medical Image Analysis*, vol. 1, no. 1, pp. 35–51, 1996.

[4] C. Studholme, D. L. G. Hill, and D. J. Hawkes, "An overlap invariant entropy measure of 3D medical image alignment," *Pattern Recognition*, vol. 32, no. 1, pp. 71–86, Jan 1999.

[5] D. Rueckert, L. I. Sonoda, C. Hayes, D. L. G. Hill, M. O. Leach, and D. J. Hawkes, "Nonrigid registration using free-form deformations: Application to breast MR images," *IEEE Transactions on Medical Imaging*, vol. 18, pp. 712–721, 1999.

[6] J. P. W. Pluim, J. B. A. Maintz, and M. A. Viergever, "Mutual information based registration of medical images: A survey," *IEEE Transaction on Medical Imaging*, vol. 22, no. 8, pp. 986–1004, 2003.

[7] X. Zhuang, D. J. Hawkes, and S. Ourselin, "Unifying encoding of spatial information in mutual information for nonrigid registration," in *Information Processing in Medical Imaging, Proceedings*, ser. Lecture Notes in Computer Science (LNCS), vol. 5636, 2009, pp. 491–502.

[8] ——, "Spatial information encoded mutual information for nonrigid registration," in *International Workshop on Biomedical Image Registration, Proceedings*, ser. Lecture Notes in Computer Science, vol. 6204, 2010, pp. 246–257.

[9] G. Hermosillo, C. Chefd'Hotel, and O. D. Faugeras, "Variational methods for multimodal image matching," *International Journal of Computer Vision*, vol. 50, no. 3, pp. 329–343, 2002.

[10] S. Klein, U. A. van der Heide, I. M. Lips, M. van Vulpen, M. Staring, and J. P. W. Pluim, "Automatic segmentation of the prostate in 3d MR images by atlas matching using localized mutual information," *Medical Physics*, vol. 35, no. 4, pp. 1407–1417, 2008.

[11] C. Studholme, C. S. Drapaca, B. Iordanova, and V. Cardenas, "Deformation-based mapping of volume change from serial brain MRI in the presence of local tissue contrast change," *IEEE Transactions on Medical Imaging*, vol. 25, no. 5, pp. 626–639, 2006.

[12] D. Loeckx, P. Slagmolen, F. Maes, D. Vandermeulen, and P. Suetens, "Nonrigid image registration using conditional mutual information," in *Information Processing in Medical Imaging, Proceedings*, LNCS, vol. 4584, pp. 725–737, 2007.

[13] ——, "Nonrigid Image Registration Using Conditional Mutual Information," *IEEE Transactions on Medical Imaging*, vol. 29, no. 1, pp. 19–29, 2010.

[14] J. P. W. Pluim, J. B. A. Maintz, and M. A. Viergever, "Interpolation artefacts in mutual information-based image registration," *Computer Vision and Image Understanding*, vol. 77, no. 2, pp. 211–232, 2000.

[15] B. Likar and F. Pernus, "A hierarchical approach to elastic registration based on mutual information," *Image and Vision Computing*, vol. 19, pp. 33–44, 2001.

[16] S. Klein, M. Staring, and J. P. W. Pluim, "Evaluation of optimization methods for nonrigid medical image registration using mutual information and B-splines," *IEEE Trans. Image Processing*, vol. 16, no. 12, pp. 2879–2890, Dec. 2007.

[17] D. Rueckert, L. I. Sonoda, C. Hayes, D. L. G. Hill, M. O. Leach, and D. J. Hawkes, "Nonrigid registration using free-form deformations: Application to breast MR images," *IEEE Transactions on Medical Imaging*, vol. 18, pp. 712–721, 1999.

[18] http://www.bic.mni.mcgill.ca/brainweb/

[19] A. Melbourne, D. Atkinson, M. J. White, D. Collins, M. Leach, and D. Hawkes, "Registration of dynamic contrast-enhanced MRI using a progressive principal component registration (ppcr)," *Physics in Medicine and Biology*, vol. 52, pp. 5147–5156, 2007.

[20] C. Li and Y. Sun, "Nonrigid registration of myocardial perfusion MRI using pseudo ground truth," in *Medical Image Computing and Computer-Assisted Intervention, Proceedings*, LNCS, vol. 5761, 2009, pp. 165–172.

[21] M. Mellor and M. Brady, "Phase mutual information as a similarity measure for registration," *Medical Image Analysis*, vol. 9, pp. 330–343, 2005.

[22] J. A. Schnabel, D. Rueckert, M. Quist, J. M. Blackall, A. D. Castellano-Smith, T. Hartkens, G. P. Penney, W. A. Hall, H. Liu, C. L. Truwit, F. A. Gerritsen, D. L. G. Hill, and D. J. Hawkes, "A generic framework for non-rigid registration based on non-uniform multi-level free-form deformations," in *Medical Image Computing and Computer-Assisted Intervention, Proceedings*, LNCS, vol. 2208, 2001, pp. 573–581.

[23] D. Rueckert, P. Aljabar, R. A. Heckemann, J. V. Hajnal, and A. Hammers, "Diffeomorphic registration using b-splines," in *Medical Image Computing and Computer-Assisted Intervention, Proceedings*, LNCS, vol. 4191, 2006, pp. 702–709.

[24] P. Thévenaz and M. Unser, "Optimization of mutual information for multiresolution image registration," *IEEE Transactions on Image Processing*, vol. 9, no. 12, pp. 2083–2099, Dec. 2000.

[25] A. Melbourne, D. Atkinson, and D. J. Hawkes, "Influence of organ motion and contrast enhancement on image registration," in *Medical Image Computing and Computer-Assisted Intervention, Proceedings, Part II*, LNCS, vol. 5242, 2008, pp. 948–955.

[26] S. Uribe, V. Muthurangu, R. Boubertakh, T. Schaeffter, R. Razavi, D. L. Hill, and M. S. Hansen, "Whole-heart cine MRI using real-time respiratory self-gating," *Magnetic Resonance in Medicine*, vol. 57, no. 3, pp. 606–613, 2007.

[27] X. Zhuang, K. Rhode, S. Arridge, R. Razavi, D. Hill, D. Hawkes, and S. Ourselin, "An atlas-based segmentation propagation framework using locally affine registration – application to automatic whole heart segmentation," in *Medical Image Computing and Computer-Assisted Intervention, Proceedings*, LNCS, vol. 5242, 2008, pp. 425–433.

[28] X. Zhuang, K. Rhode, R. Razavi, D. J. Hawkes, and S. Ourselin, "A registration-based propagation framework for automatic whole heart segmentation of cardiac MRI," *IEEE Transactions on Medical Imaging*, vol. 29, no. 9, pp. 1612–1625, 2010.